Physician-modified endograft using three-dimensional model-assisted planning

Hiroshi Mitsuoka, MD, PhD, Yasuhiko Terai, MD, *and* Yuta Miyano, MD, *Shizuoka, Japan*

ABSTRACT

Objective: Case-specific and true-to-scale three-dimensional (3D) models have become increasingly useful tools for physician-modified endovascular grafting. This study aimed to validate the use of 3D model-assisted planning for fenestration design.

Methods: Thirty-two consecutive patients (2019-2021) presenting with pararenal or juxtarenal abdominal aortic aneurysm (n = 16), paravisceral abdominal and Crawford's extent IV thoracoabdominal aortic aneurysm (n = 12), and type I endoleak after endovascular repair (n = 4) were analyzed retrospectively. All cases were planned manually with a standard method using curved planar reconstruction stretch images and multiplanar images perpendicular to the centerlines. The design was finalized by intraoperative 3D model-assisted planning. Intermethod agreements were assessed for geometrical relationships (separation heights and angles) between the superior mesenteric and renal arteries. The datasets from 55 double measurements of the entire cohort in this series were used to assess measurement discrepancies (≥3 mm separation height or ≥15° angle difference) and fenestration mismatches (≥3 mm separation between the manually planned and 3D model-assisted-planned renal arterial centers on the device surface) between manual and 3D model-assisted planning. Statistical analyses were performed to test the impact of anatomical factors on the discrepancies and mismatches. The imposition accuracy of 3D model-assisted planning and short-term clinical results of the 32 cases were also evaluated.

Results: Fourteen fenestration measurement discrepancies were detected. The size of the stent graft ($P = .0381$), the aortic angle ($P = .0008$), and the prior existence of stent graft ($P = .0123$) were found to have a statistically significant impact on the measurement discrepancy, using single logistic and Fisher's exact tests. Twelve fenestration mismatches were observed and found to be significantly affected ($P = .0039$) by aortic angle. A cutoff value for fenestration mismatch was found to be 36.5°, with a sensitivity and specificity of 69.2% and 80.5%, respectively, using receiver operating characteristic analysis (area under the curve, 0.782 ± 0.081; $P = .0023$). A high level of branch preservation (100%) was achieved. During the observation period (1.3 years on average; range, 0.5-2.5 years), no patient experienced complications related to fenestration.

Conclusions: The differences between the planning methods were non-negligible. However, 3D model-assisted planning increased the precision of the fenestration design when the conformation of the stent graft to the aortic anatomy is taken into account. (J Vasc Surg Cases Innov Tech 2022;8:794-801.)

Keywords: Abdominal aortic aneurysm; Paravisceral; Juxtarenal; Fenestrated endovascular aneurysm repair; Simulation

Fenestrated endovascular repair is an established treatment for aortic aneurysms with complex anatomy.[1,2] Although various commercial devices have been developed, physician-modified endoluminal grafts (PMEG) are used frequently worldwide owing to restrictions in regional availability or time limits for urgent procedures. With the recent trend of personalized medicine and rapidly evolving three-dimensional (3D) printing technologies, it was natural that 3D models become increasingly useful tools for PMEG fenestration designing.[3-8] However, new technologies in their nascent stage may hold pitfalls for the unwary, and there remains a lack of data to validate the 3D model-assisted (3DMA) planning method. Intermethod agreements with standard measurements have not been investigated, and the accuracy has been appreciated on a case-report basis. This study estimates the impact of aortic anatomy on discrepancies between manual and 3DMA planning. The imposition accuracy of 32 cases was also evaluated. The study aimed to validate the use of 3DMA planning for complex aortic pathologies treated with PMEG.

METHODS

Thirty-two consecutive patients with PMEG (n = 32; March 2019 to September 2021) who presented with

From the Vascular and Endovascular Center, Department of Cardiovascular Surgery, Shizuoka City Shizuoka Hospital.

Sponsored partially by the "Industrial Cluster Project of Shizuoka Prefecture" from the Shizuoka prefectural business development office.

Author conflict of interest: none.

Correspondence: Hiroshi Mitsuoka, MD, PhD, Vascular and Endovascular Center, Department of Cardiovascular Surgery, Shizuoka City Shizuoka Hospital, 10-93 Ote-machi, Aoi-ward, Shizuoka City, 420-8630, Japan (e-mail: hiroshimitsuoka@mac.com).

The editors and reviewers of this article have no relevant financial relationships to disclose per the Journal policy that requires reviewers to decline review of any manuscript for which they may have a conflict of interest.

2468-4287

https://doi.org/10.1016/j.jvscit.2022.10.012

pararenal or juxtarenal abdominal aortic aneurysm (n = 16), paravisceral abdominal and Crawford's extent IV thoracoabdominal aortic aneurysm (n = 12), and type I endoleak after endovascular repair (n = 4) were included in this study. None of the patients were considered eligible for open repair (American Society of Anesthesiologists class 3). In Japan, PMEG was listed as one of "the new medical technologies with the highest difficulties" in 2017 and was prescribed by The Ordinance for the Enforcement of National Medical Acts. The practice was advised in accordance with the "Guidelines for Nationally Registered Specific Functional or Core Hospitals." The practice and study protocols were approved by an institutional ethical review board in 2017, and the practice appropriateness was further discussed on a case-by-case basis in a multidisciplinary conference involving anesthesiologists, cardiologists, cardiovascular and endovascular surgeons, nurses, and clinical medical engineers. Written informed consent for the procedure and publication consent were obtained from all patients. After the procedure, patients were monitored using clinical and imaging data at the 30-day, 3-month, and 6-month marks as well as every 6 months thereafter.

Image analysis and manual planning. Osirix MD (Pixmeo SARL, Bernex, Switzerland) was used for manual planning and image analyses. The axial slice thickness of the computed tomography (CT) scan was limited to 0.625 mm. To evaluate intermethod agreements, the interpretational errors of the ostial centers must be minimized.[9,10] Therefore, the ostial center of the celiac arteries, superior mesenteric artery (SMA), and right and left renal arteries were marked in the volume data and referenced as the branch ostial center points in all planning methods.

For manual planning using curved planar reconstruction images with a centerline on the axis (CPR planning), a semiautomated central lumen line was created by placing seed points on the most proximal part of the descending aorta and below the common iliac artery, which was used for main body access. The centerline generated by the workstation was accommodated to simulate the centerline of the device conforming to aortic anatomy.[11] A stretch view was used to measure the vessel separation heights. The longitudinal branch separation (height separation) was defined as the distance between the planes, including the reference points of each branch ostium. The results are expressed in millimeters with values rounded to the nearest whole number. The separation angle of the target vessel ostia was measured in the axial image that included the same plane, and the results were rounded to the nearest integer. Separation heights (millimeters) and angles (0°-180°) of the branches were standardized to SMA (0 mm, 0°) (Fig 1, *left*).

3DMA planning. A 3D printer (Form 2, Formlabs Inc., Somerville, MA) and CAD creator (Mimics InPrint 3.0, Materialize NV, Leuven, Belgium) were used.[7] The range of 3D segmentation included at least 5 cm above the most proximal target vessel through the terminal aorta. The branch center points were also referenced for 3DMA planning, and branch windows of the hollow transparent 3D model were created such that these reference points were included in the center of the window.

The models were created in an aseptic condition, where the resin was photopolymerized by ultraviolet light. The residual resin on the surface was vigorously washed with 100% ethanol, after which the models were further cured with ultraviolet light at 60°C. Next, the models were sterilized using ethylene oxide (ETO), a proven method for sterilizing surgical instruments in our institute that does not require high temperatures like autoclave sterilization methods. Because the models were hollowed out, ETO contacted the entire surface efficiently. The models were exposed to ETO for 2 h at 60°C. Aeration before packaging took approximately 24 h at 60°C.

All cases were initially designed manually. Devices were chosen such that the fenestrations could be designed without interference from stent struts. Temporary or permanent diameter-reducing sutures were not constructed in these cases. On the back table of the procedures, a few stent segments of the endograft were extruded from the deployment sheath. The manually planned SMA fenestration center was marked on the surface of the device using a noncarcinogenic skin marker. The device was resheathed, and then deployed inside the 3D model with SMA centers superimposed on each other. The stent graft was further deployed until the position of the fenestrated segment was stabilized inside. The other fenestration centers were marked with the skin marker, and the positions of the markers were recorded after dismantling the model. The results of 3DMA planning were adopted as the final design (Fig 2). Fenestrations were created using ophthalmic cautery and reinforced with 4-0 Ethibond sutures (Ethicon, Johnson & Johnson Company, Somerville, NJ) and a platinum microcoil (IDC 18, Boston Scientific, Marlborough, MA). The recorded images were used to translate the results into comparable datasets (Fig 1, *right*).

3D image-guided deployment process. Contrast-enhanced cone beam CT scans were performed after the deployment sheath was inserted. The centers of the branch openings were marked three-dimensionally, and the device was deployed until the index fenestration was superimposed onto the corresponding targeted branch opening. SMA fenestration was used as an index fenestration (Fig 3) except in cases where it was not present. The device could be rotated and repositioned

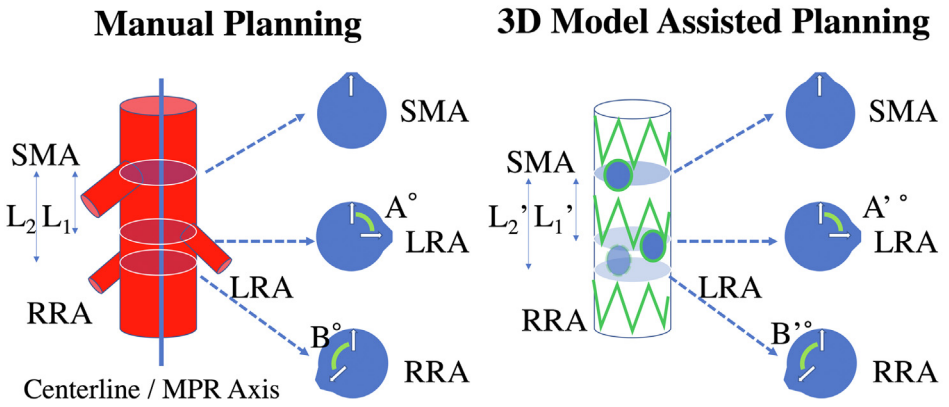

Fig 1. Geometric relations among SMA, RRA, and LRA. **(Left)** L1 and L2 are defined as the distances between the planes, including the reference points of the branches. A° and B° were standardized to SMA (0°). **(Right)** The fenestration centers are marked on the endograft surface in the three-dimensional (*3D*) model. The marked device was photo-recorded to translate the results into comparable forms of datasets (L1', L2', A'°, and B'°). *LRA*, left renal artery; *RRA*, right renal artery; *SMA*, superior mesenteric artery.

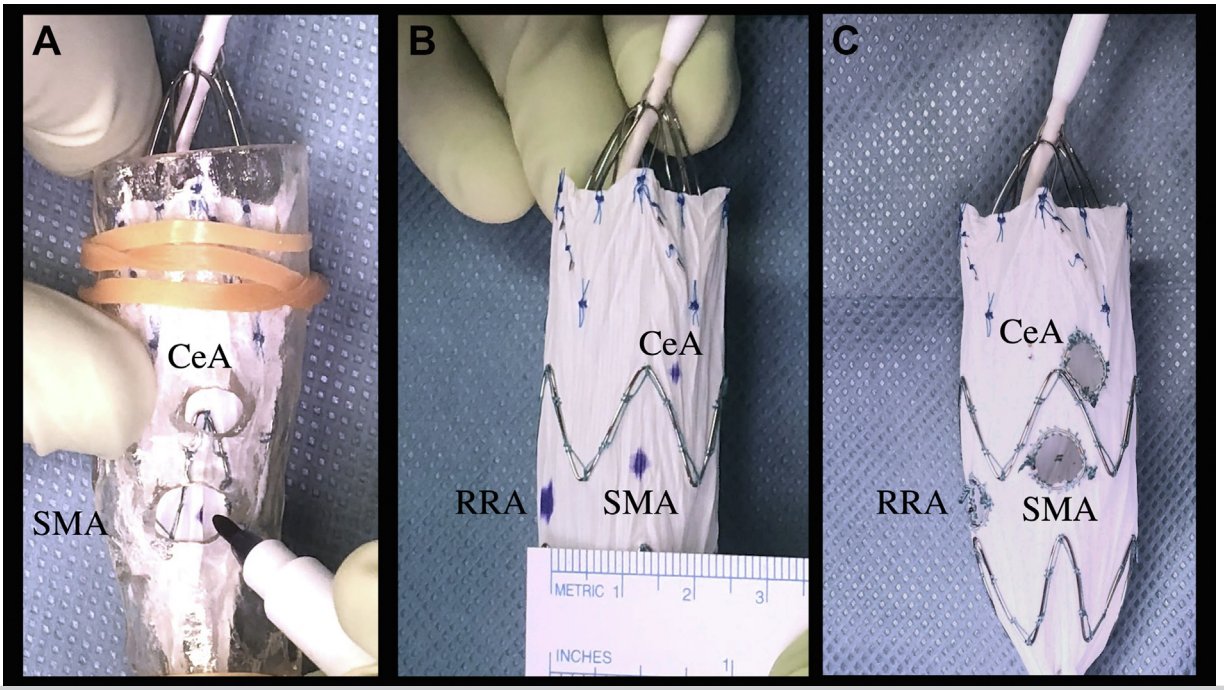

Fig 2. Three-dimensional (3D) model-assisted measurement (3D-MA). The device was deployed inside the 3D model **(A)**. Geometrical relationships among the fenestration centers were measured after dismantling the model **(B)**. The results of 3DMA planning were adopted as the final design **(C)**. *CeA*, celiac artery; *RRA*, right renal artery; *SMA*, superior mesenteric artery.

before the first three stent segments were deployed completely from the delivery sheath.

Impact of aortic anatomy on fenestration design discrepancy. Two patients underwent single renal arterial fenestrated PMEG implantation. In these patients, 3DMA planning was used for the maximum use of the proximal sealing zone. In one patient, the SMA and celiac artery were targeted, but the renal arteries were sacrificed bilaterally because the patient had terminal-stage renal disease and was dependent on hemodialysis. Three other patients required SMA and single renal arterial fenestrations because the other kidney was nonfunctional or because they had a previous history of unilateral nephrectomy. Consequently, 55 paired sets of geometric relations between SMAs and renal arteries in

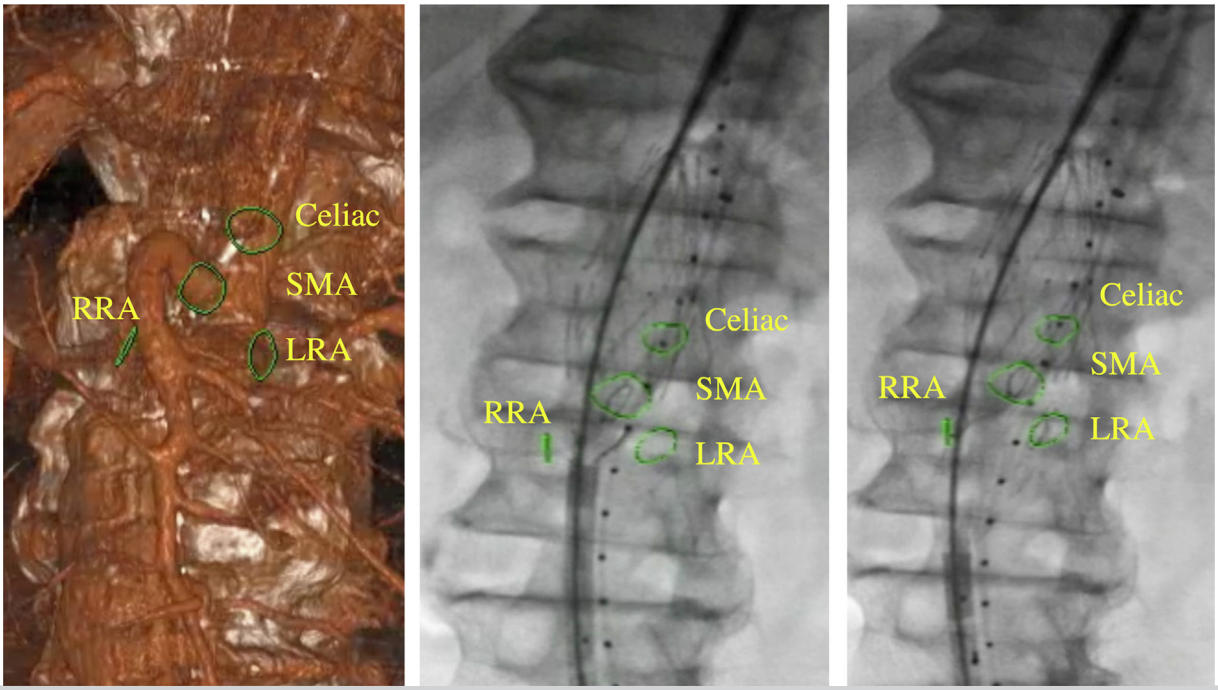

Fig 3. Three-dimensional (3D) image-aided deployment process. **(Left)** A volume-rendering image of cone-beam computed tomograph scan performed with the deployment sheath inserted. The branch ostia, including the celiac arteries (*Celiac*), are marked with green circles. **(Center)** The SMA fenestration was initially superimposed. **(Right)** The device was further deployed to optimize matching of the LRA and RRA. *LRA*, left renal artery; *RRA*, right renal artery; *SMA*, superior mesenteric artery.

29 PMEG cases were available to compare manual and 3DMA planning.

The size of the renal fenestration was uniformly 6 mm in diameter, and a height measurement difference of 3 or more mm resulted in a less than 50% overlap of the fenestration areas of manual and 3DMA planning measurements. Likewise, a separation angle difference 15° or more on the 24-mm diameter of the aorta, which was the average size of the aortic endoluminal diameter at the lowest renal arterial level in this series, caused the same level of overlap (small) and coinciding agreement. Therefore, a separation angle 15° or more or a height difference 3 mm or more was considered a significant preoperative measurement discrepancy. If there was a 3 mm or greater separation between the manually planned and 3DMA-planned renal arterial centers on the device surface, it was considered a fenestration mismatch.

The influence of anatomical factors, which theoretically influence measurement discrepancies and fenestration mismatches, was statistically tested. The factors considered were suprarenal complexity (SRC), the number of stents above the lowest renal artery, the maximum oversizing and size of the stent graft, the aortic angle between the suprarenal aorta and aneurysmal axis,[12] and the existence of a previous stent graft (yes = 1, no = 0). SRC was quantified by calculating the tortuosity as follows:

$$\text{SRC} = \text{Lc}/\text{Ld}$$

where Lc is the height separation between the lowest renal and celiac arteries along the adjusted centerline, and Ld is the linear distance between the center points on the centerline axial images, including the reference points for the celiac and lowest renal arteries.

Perioperative and short-term results. Procedural (index procedure) and postoperative data (collected on the 30-day, 3-month, and 6-month marks and every 6 months thereafter) were collected. Postoperative survival, major adverse events, primary and assisted patency of renal stents, sac shrinkage (proportion of cases exhibiting a maximum-minimum aneurysmal diameter of >5 mm), and sac stability (proportion of cases not exhibiting a >5-mm increase in the maximum-minimum aneurysmal diameter) were evaluated. The patency of targeted vessels was mainly assessed using contrast CT scans. Follow-up imaging was performed for two patients using CT scans without contrast and duplex ultrasound examination because the use of contrast agent was contraindicated in them.

Table I. Single logistic regression analyses and Fisher's exact test of anatomical factors affecting design discrepancy

Explanatory variables	Value or mean ± SD (range)	Odds Ratio	95% CI	*P* value
Suprarenal complexity	1.08 ± 0.06 (1.00 to 1.23)	4.197	0.0002317-60613	.7677
No. of stents	2.62 ± 0.55 (2 to 4)	0.128	-0.820 to 1.145	.7944
Maximal oversizing, %	40.5 ± 17.9 (13.4 to 89.4)	7.993	0.271-271.0	.2277
Size of stent graft, mm	31.3 ± 4.3 (24 to 38)	1.188	1.020-1.421	.0381
Aortic angle, degrees	29.2 ± 18.6 (4 to 71)	1.087	1.041-1.150	.0008
Previous EVAR (1 or 0)	Not calculated	6.286	1.641-21.98	.0121

CI, Confidence interval; *EVAR*, endovascular repair; *SD*, standard deviation.

Table II. Single logistic regression and Fisher's exact test of anatomical factors affecting fenestration mismatch

Explanatory variables	Value or mean ± SD (range)	Odds Ratio	95% CI	*P* value
Suprarenal complexity	1.08 ± 0.06 (1.00-1.23)	1.918	0.0002317-60,613.0000000	.7677
No. of stents	2.62 ± 0.55 (2-4)	0.938	0.3346-2.7090	.8975
Maximal oversizing, %	40.5 ± 17.9 (13.4-89.4)	2.08	0.0406-79.5000	.697
Size of stent graft, mm	31.3 ± 4.3 (24-38)	1.088	0.940-1.278	.2714
Aortic angle, degrees	29.2 ± 18.6 (4-71)	1.061	1.022-1.110	.0039
Previous EVAR (1 or 0)	Not calculated	3.036	0.7713-0.1110	.111

CI, Confidence interval; *EVAR*, endovascular repair; *SD*, standard deviation.

Statistical analyses. Data were anonymized after measurements and handled in a single-blinded manner. Statistical analyses were performed using Prism 9 software (version 9.3.1; GraphPad Software, San Diego, CA). A *P* value of less than .05 was considered statistically significant.

RESULTS

Impact of anatomic factors on design discrepancy. Fourteen fenestration measurement discrepancies were detected. Single-logistic analysis and Fisher's exact testing showed a statistically significant impact from the size of the stent graft ($P = .0381$), aortic angle ($P = .0008$), and the prior stent graft existence ($P = .0123$; Table I). Twelve fenestration mismatches were observed; the single logistic analysis and Fisher's exact test found a statistically significant impact from the aortic angle ($P = .0039$; Table II). Receiver operating characteristic analysis revealed an aortic angle of 36.5o as the cutoff value for fenestration mismatch (area under the curve, 0.782 ± 0.081; $P = .0023$), with a sensitivity and specificity of 69.2% and 80.5%, respectively.

Clinical results. The demographics of the patients are listed in Table III. The distribution of fenestrations, branch artery stenting, and the types of physician-modified main body endograft are listed in Table IV. All patients underwent successful fenestrated device implantation. Self- or balloon-expandable bare stents were used to prevent window shuttering or migration of the main device. Covered stents were used if the sealing ability was to be implemented. Finally, 57 renal fenestrations were created, which were stented with five Viabahn self-expandable stent grafts (VSX, W. L. Gore & Associates, Flagstaff, AZ), 47 balloon-expandable Viabahn VBX stent grafts (VBX, W. L. Gore & Associates), and 5 bare balloon-expandable stents (Express SD, Boston Scientific, Bloomington, MN). Nine covered (one VSX and eight VBX) and 15 self-expandable (S.M.A.R.T Flex, Cardinal Health, Dublin, OH) stents were used as bridging stents for the SMA. Two covered stents (VBX) were used for celiac fenestrations. Neither type I nor III endoleaks were observed postoperatively. All branches were preserved successfully and remained patent during the observation period. The average observation period for the 32 patients was 1.3 years (range, 0.5-2.5 years). No patient experienced sac enlargement. Sac shrinkage was observed in 15 cases. Kaplan-Meier analysis showed a satisfactory level of cumulative sac shrinkage occurrence (>5 mm shrinkage; 95% confidence interval, 53.6 ± 9.9%; numbers at risk, year 0 = 32, year 1 = 12) at postoperative year 1.

DISCUSSION

Fenestration is designed based on the hypothesis that perioperative aortic deformation is negligible and that the geometric relations of branch openings are accurately reproduced on the modified device surface. During the image-guided deployment process, the index fenestrations were superimposed initially, and the alignment of the others was optimized stepwise. Therefore, this study highlights the importance of evaluating the geometric relationship between fenestrations and not

Table III. Demographics of the patients

Demographics	No. (%) or mean ± SD (range)
Age, years	75.6 ± 6.8 (60-89)
Male sex, %	30 (93.8)
Smoking history	31 (96.8)
Coronary artery disease	16 (50)
Congestive heart failure	10 (31.3)
Diabetes mellitus	5 (15.6)
Hypertension	32 (100)
Chronic obstructive pulmonary disease	14 (43.7)
Hyperlipidemia	11 (34.3)
ASA class ≥3	32 (100)

ASA, American Society of Anesthesiologists' Physical Status Classification; *SD*, standard deviation.

Table IV. Distribution of fenestrations, endografts, and branch artery stents

	No.	Stented (%)
Celiac fenestrations	23	2 (10)
SMA fenestrations	30	29 (96.6)
Renal fenestrations	57	57 (100)
Modified devices		
Cook Zenith Flex	7	
Medtronic Valiant	1	
Cook TX2	2	
Cook Zenith Alpha Thoracic	21	
Cook Zenith Alpha Abdominal	1	
Fenestrations per patient (average)	3.1	

SMA, Superior mesenteric artery.

the geometry of each fenestration itself. Only geometric relations between the SMA and renal arteries were evaluated, as celiac fenestrations in many cases were designed as large (≥8 mm) fenestrations without stent struts.

In this series of patients, the devices were chosen such that the fenestrations were created on the surface of the devices without interference from stent-struts. Zenith Flex (Cook Medical LLC, Bloomington, IN) had been used predominantly, because it is easily resheathed. In the early phase, when the average number of fenestrations per case was approximately two, multiple fenestration procedures were limited so that the stent struts did not interfere with the locations of the fenestration. However, as more fenestrations (>3) became favorable for later cases, Valiant (Medtronic Vascular, Santa Rosa, CA) and then Zenith alpha thoracic (Cook Medical LLC) were chosen.

Although opinions may differ between centers, we did not prepare permanent or temporary diameter-reducing ties and wires, because they may damage the integrity of the stent grafts and interfere with deployment processes. In our hands, before the first three stent segments were completely deployed from the delivery sheath, the fenestrated devices could be rotated and repositioned without difficulty. The second stent graft segment (the first segment with graft) was also constrained to some extent before this stage. Usually, this segment is 15% to 30% larger than the aortic diameter with respect to the device's instruction for use. Because we did not include branch type cases in this study, the fenestrations made full contact with the aortic inner surface, and the averaged maximum oversizing in the fenestrated segment in our study resulted in a higher range.

A non-negligible difference was observed between CPR and 3DMA planning. Such variability reportedly arises from the subjective interpretation of anatomical landmarks.[9,10] This study minimized the subjectivity effect by referencing the same landmarks for all measurement methods. However, the effect of subjectivity could not be removed completely because the centerlines were created and adjusted based on the experience of a single planner. Regression analyses identified a statistically significant impact of infrarenal aortic angulation on measurement discrepancies and fenestration mismatches. If the PMEG was designed for an aorta with a straight anatomy, there would be a higher level of agreement in measurements. However, the effect of aortic angulation on the device adaptation is difficult to measure and design using manual measurement from image data. Planning with 3DMA incorporates the ability to consider the adaptation of the device to the anatomy; this is achieved by graft wrinkling and uneven stent strut opening (Fig 4). Therefore, intermethod variabilities between manual and 3DMA plannings originate from the measurement principles and do not appear to be solely caused by subjective interpretation differences.[9,10]

It should be noted that aortic angulation may thus influence measurement. In fact, in vivo malalignment is often observed in renal arterial fenestrations around the curvature,[4] and we also experienced a similar imposing failure of left renal artery before employing 3DMA planning. The definitions of design discrepancy and fenestration mismatch in this study may not directly lead to branch preservation failure, as branch shuttering may be recovered even in some challenging situations of designing or positioning errors.[13] However, this inaccuracy may cause mid- to long-term branch or fenestration-related failures, which manifest as shuttering, bridging stent deformation, and branch occlusion.[10]

When applied to severely curved cases, 3DMA planning using nonconformable templates loses accuracy.[10,14] Under such circumstances, perioperative aortic deformation caused by the device-aorta interaction must be

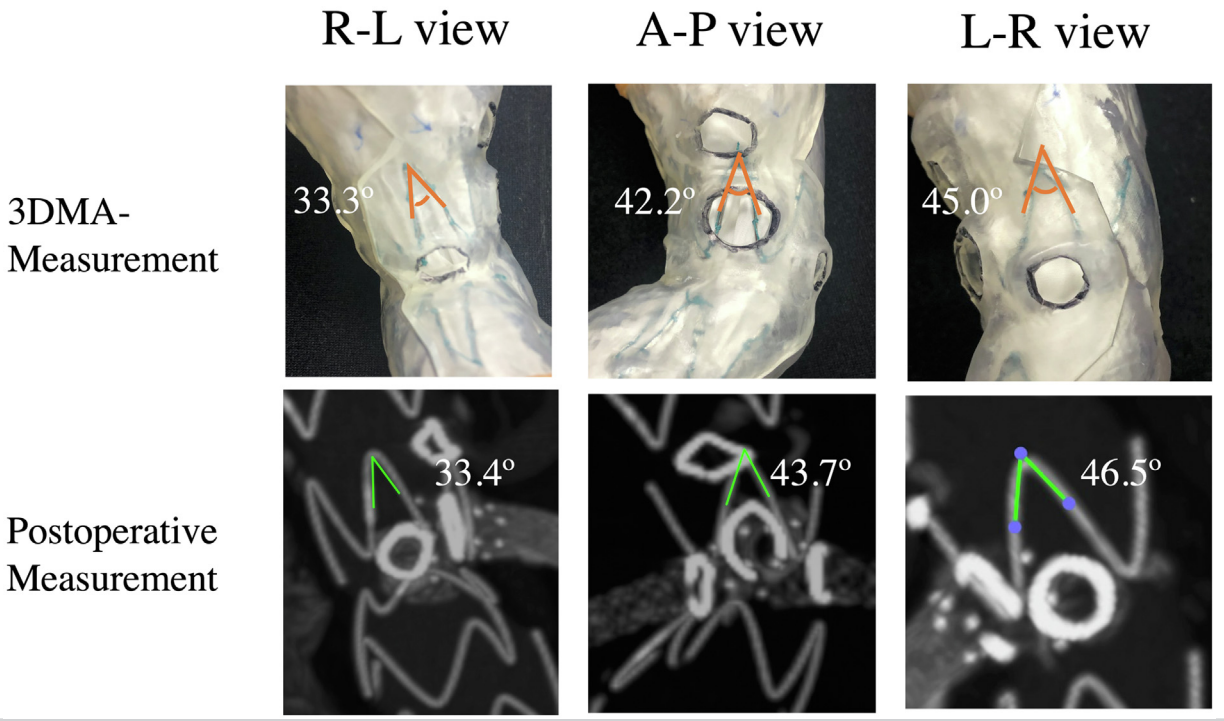

Fig 4. Adaptation of stent graft to aortic curvature. A thoracic stent graft was deployed in the juxtarenal abdominal aortic aneurysm with severe infrarenal aortic curvature. Pictures of 3D model-assisted (*3DMA*) **(top)** and postoperative measurement **(bottom)** are shown. Note the uneven levels of stent strut opening above the renal arteries. *A-P*, anteroposterior; *L-R*, lateral view seen from the left to right; *R-L*, the right to left.

considered. The flexible 3D template may partially simulate aortic conformation,[14] but the interaction occurs through a more complex process, including surrounding tissue reactions and local hemodynamics. Fenestration complications beyond this observation period may be affected by postoperative remodeling.[10,15,16] Further follow-up is mandatory, and future planning methods should consider perioperative aortic deformation and postoperative remodeling.

CONCLUSIONS

There were non-negligible differences between manual and 3DMA planning methods. However, when considering the conformation of the stent graft to the aortic anatomy, 3DMA planning increased the precision of the fenestration design.

REFERENCES

1. Oderich GS, Ribeiro M, Hofer J, Wifham J, Cha S, Chini J, et al. Prospective, nonrandomized study to evaluate endovascular repair of pararenal and thoracoabdominal aortic aneurysms using fenestrated-branched endografts based on supraceliac sealing zones. J Vasc Surg 2017;65:1249-59.
2. Motta F, Oderich GS, Tenorio ER, Schanzer A, Timaran CH, Schneider D, et al. Fenestrated-branched endovascular aortic repair is a safe and effective option for octogenarians in treating complex aortic aneurysm compared with nonoctogenarians. J Vasc Surg 2021;74:353-62.
3. Huang J, Li G, Wang W, Wu K, Le T. 3D printing guiding stent graft fenestration: a novel technique for fenestration in endovascular aneurysm repair. Vascular 2017;25:442-6.
4. Starnes BW, Tatum B, Singh N. Procedural and perioperative results in patients treated with fenestrated endovascular aneurysm repair planned by automated software in a physician-sponsored investigational device exemption trial of physician-modified endografts. J Vasc Surg 2018;68:1297-307.
5. Branzan D, Schmidt A, Winkler D, Scheinert D, Grunert R. EVAR in 3D: the Leipzig experience. Endovasc Today 2019;18:93-6.
6. Barón Vladimir, Guevara Romeo. Three-dimensional printing-guided fenestrated endovascular aortic aneurysm repair using open source software and physician-modified devices. J Vasc Surg Cases Innov Tech 2019;5:566-71.
7. Mitsuoka H, Terai Y, Miyano Y, Naito N, Tanai J, Kawaguchi S, et al. Preoperative planning for physician-modified endografts using a three-dimensional printer. Ann Vasc Dis 2019;12:334-9.
8. Mafeld S, Nesbitt C, McCaslin J, Bagnall A, Phillip D, Bose P, et al. Three-dimensional (3D) printed endovascular simulation models: a feasibility study. Ann Transl Med 2017;5:42-9.
9. Oshin OA, England A, McWilliams RG, Brennan JA, Fisher RK, Vallabhaneni SR. Intra- and interobserver variability of target vessel measurement for fenestrated endovascular aneurysm repair. J Endovasc Ther 2010;17:402-7.
10. Koleilat I, Jaeggli M, Ewing JA, Androes M, Simionnescu DT, Eirt J. Interobserver variability in physician-modified endograft planning by comparison with a three-dimensional printed aortic model. J Vasc Surg 2016;64:1789-96.
11. Simons JP, Schanzer A. Ten Steps-A standardized 10-step approach to the planning and sizing of a fenestrated endovascular aortic aneurysm repair. Endovasc Today 2017;16(Suppl):8-10.
12. Keulan JW, Moll FL, Tolenaar JL, Verhagen HJ, van Herwaarden JA. Validation of a new standardized method to measure proximal aneurysm neck angulation. J Vasc Surg 2010;51:821-8.

13. Oderich GS, Tenorio E, Sandri G. Recommendations from a busy fenestrated practice. Endovasc Today 2017;16(Suppl):15-20.
14. Coles-Black J, Barber T, Chuen J. A flexible 3D printed template to assist with physician modified endografts for FEVAR. Euro J Vasc Endovasc Surg 2021;61:699-700.
15. Ullery BW, Lee GK, Lee JT. Shuttering of the superior mesenteric artery during fenestrated endovascular aneurysm repair. J Vasc Surg 2014;60:900-7.
16. Verhoeven EL, Vourliotakis G, Bos WTGJ, Tielliu IFJ, Zeebregts CJ, Prins TR, et al. Fenestrated stent grafting for short-necked and juxtarenal abdominal aortic aneurysm: an 8-year single-center experience. Eur J Vasc Endovasc Surg 2010;39:529-36.

Submitted Jul 15, 2022; accepted Oct 19, 2022.